
Domain Knowledge Infused Conditional Generative Models for Accelerating Drug Discovery

Bing Hu

Computer Science
University of Waterloo
b25hu@uwaterloo.ca

Jong-Hoon Park

Department of Software
Yonsei University
jonghoon_park@yonsei.ac.kr

Anita Layton

Applied Math
University of Waterloo
a21ayton@uwaterloo.ca

Young-Rae Cho

Department of Software
Yonsei University
youngcho@yonsei.ac.kr

Sun Sun

National Research Council
University of Waterloo
sun.sun@uwaterloo.ca

Helen Chen

Public Health Sciences
University of Waterloo
helen.chen@uwaterloo.ca

Abstract

The role of Artificial intelligence (AI) is growing in every stage of drug development. Nevertheless, a major challenge in drug discovery AI remains: Drug pharmacokinetic (PK) and Drug-Target Interaction (DTI) datasets collected in different studies often exhibit limited overlap, creating data overlap sparsity. Thus, data curation becomes difficult, negatively impacting downstream research investigations in high-throughput screening, polypharmacy, and drug combination. We propose xImagand-DKI, a novel SMILES/Protein-to-Pharmacokinetic/DTI diffusion model capable of generating an array of PK and DTI target properties conditioned on SMILES and protein inputs that exhibit data overlap sparsity. We apply domain knowledge integration (DKI) with additional molecular and genomic domain knowledge from the Gene Ontology and molecular fingerprints to further improve our model performance. We show that xImagand-DKI generates synthetic PK data that closely resemble real data univariate and bivariate distributions, and can adequately fill in gaps among PK and DTI datasets. As such, xImagand-DKI is a promising solution for data overlap sparsity and may improve performance for downstream drug discovery research tasks. Our code and data are available open-source <https://github.com/GenerativeDrugDiscovery/xImagand-DKI>.

1 Introduction

Artificial intelligence (AI) is set to substantially reduce the \$2-3 billion dollars and 10-15 years typically required to bring a drug candidate to market [1, 2]. Fewer than 10% of drug candidates successfully reach the market [2], with the vast majority failing in clinical development due to safety and lack of or insufficient activity [3]. AI is gaining momentum in drug discovery by enabling innovative preclinical approaches, including target selection and identification [4], drug repurposing [5, 6], drug-target interactions (DTI) [7], drug property prediction [1], de novo generation [8, 9], and synthetic data generation [10].

These advances in AI-driven drug discovery has been fueled by ongoing efforts to promote open access to data for AI training and testing [11-13]. Despite the growing availability of diverse datasets, limited overlap among them presents challenges for research questions that require data integration from multiple datasets [14]. Given that data collection for drug discovery through assay panels is

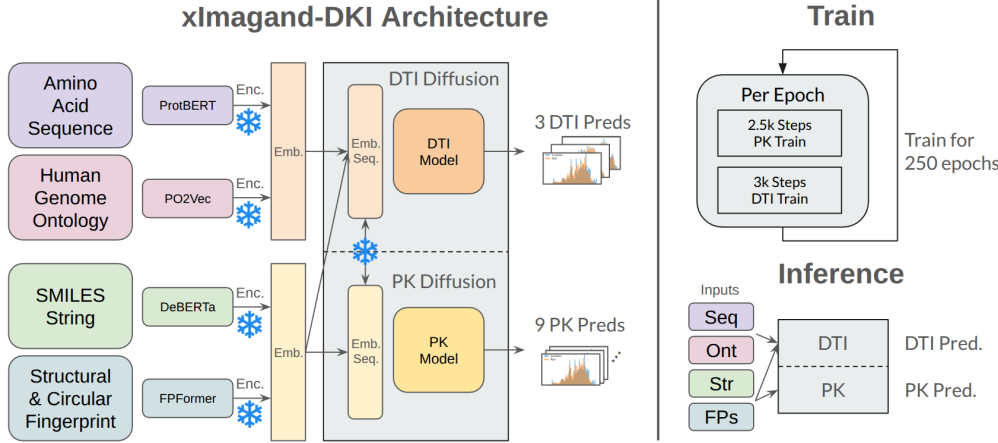


Figure 1: The xImagand-DKI architecture, training, and inference methodology. Embeddings for proteins and SMILES are generated using ProtBERT and DeBERTa, respectively. Protein knowledge infusion from the human Gene Ontology (GO) is generated using PO2Vec, and SMILES knowledge infusion from fingerprints is generated using FPFormer. The model undergoes 2.5k PK training steps and 3k DTI training steps every epoch.

both expensive and time-consuming, synthetic drug discovery data emerges as a promising alternative solution.

Recent advances in AI for drug discovery have leveraged Denoising Diffusion Probabilistic Models (DDPMs) [15], a new class of diffusion models capable of generating ligand structures [8, 16–18]. Emerging research has demonstrated that diffusion models can also generate pharmacokinetic (PK) properties [10], and when integrated into a ligand diffusion pipeline [9]. However, sequence-based molecular and biological representations, such as SMILES and amino acid sequences, alone are likely not sufficient in fully capturing the complexity of natural entities like drug molecules, proteins, and omics data. By fusing multiple views of the same molecule or profile, multi-view representation approaches for molecules [19] and omics profiles [20] can yield unified representations with enhanced predictive power.

Motivated by these advances, we present xImagand-DKI, a novel multi-view SMILES/Protein-to-PK/DTI (SP2PKDTI) diffusion model. Conditioned on SMILES and protein embeddings, xImagand-DKI is capable of simultaneously generating 12 PK properties and 3 DTI values. Our key contributions are as follows:

- Proposes an end-to-end framework that unifies PK property prediction and DTI modeling into a single foundational model, advancing solutions to data overlap sparsity by generating high-quality synthetic drug discovery data.
- Introduces multi-view domain knowledge integration (DKI) methods that incorporate protein knowledge from the Gene Ontology (GO) [21] and various molecular fingerprints
- Demonstrates how end-to-end training method combined with multi-view DKI can effectively address the challenge of data overlap sparsity, bridging the gap between PK and DTI datasets.

Notably, xImagand-DKI generates dense synthetic data that addresses the challenges posed by sparse and non-overlapping PK and DTI datasets. Using xImagand-DKI, researchers can generate large synthetic PK and DTI assay data across thousands of ligands, enabling the exploration of polypharmacy and drug combination research questions, at a fraction of the cost of conducting *in vitro* or *in vivo* PK assay panels.

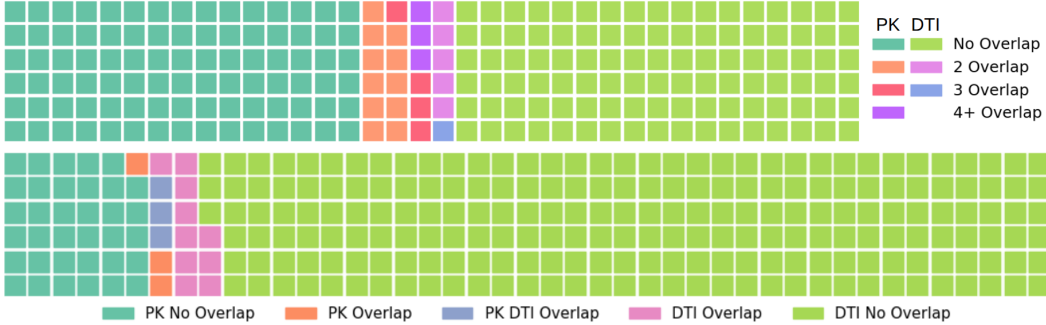


Figure 2: Visualizing data overlap sparsity between PK datasets and between DTI datasets (top), and between PK and DTI datasets (bottom). When compared to the total size of DTI and PK data points, 700k and 17k, respectively, we see data overlap sparsity, with a small percentage of molecules that belong to at least two datasets. We observe 16% of PK and 4.7% of DTI molecules with overlap.

Dataset	Caco.	Lipo.	AqSo.	Free.	PPBR	VDss	Half	CIH	CIM	Total
DTI Overlap	338	2789	1189	112	1241	184	486	698	794	4883
PK Overlap	179	1751	884	527	1296	163	337	879	1018	2772
Dataset Size	906	4200	9982	642	1797	1111	665	1020	1102	17k

Table 1: Number of overlapping molecules for each 9 PK dataset with DTI and other PK datasets. We observe that there is a greater number of unique molecules in PK datasets that overlap with DTI datasets compared to other PK datasets.

2 Background

Diffusion methods leverage families of probability distributions to model complex datasets in a way that enables computationally tractable learning, sampling, inference, and evaluation [16]. DDPM [15] operates by first systematically destroying the structure in the data through a forward process, and then learning to reconstruct it from noise via a reverse generative process. Recent literature has highlighted significant advances in the use of diffusion models for small-molecule generation [8, 22–24], conditional generation of drug PK properties [9, 10], and multi-view fusion for DTI prediction [19, 25, 26]. In this study, we propose xImagand-DKI, a unified multi-view approach that leverages both molecular and protein perspectives for synthetic data generation in drug property and DTI prediction. Specifically, xImagand-DKI integrates molecular multi-views through circular and structural molecular fingerprints, and protein multi-views using omics relationships derived from the GO.

2.1 Drug Discovery Data Overlap Sparsity

Drug discovery fails for two main reasons [27]: lack of efficacy and safety concerns. Understanding the relationship between solubility, toxicity, molecular structure, and drug response is essential for effective drug development [28, 29], as these properties play a critical role in shaping a compound’s absorption, distribution, metabolism, excretion, and Toxicity (ADMET) profile, as well as its therapeutic window and overall clinical viability. In this work, xImagand-DKI is trained to conditionally generate both drug properties and DTI data, addressing these challenges through a unified framework.

PK broadly describes what the body does to a drug, encompassing absorption (how the drug is taken up into the body), bioavailability (the extent to which the active drug enters systemic circulation), distribution (how the drug spreads through tissues), metabolism (how the body breaks down the drug), and excretion (how the drug is removed from the body). Issues related to PK properties are among the primary causes for compound attrition in small-molecule drug development [30], making accurate PK computational tools increasingly vital; and recent advances have significantly improved their capabilities [31–33].

DTI prediction examines the relationships between drugs and their biological targets, providing insights into the molecular pathophysiology of diseases [1, 34]. Accurately modelling DTI is crucial for applications such as drug repurposing, high-throughput screening, lead optimization, polypharmacy and drug combination research [1]. Extending PK profiling across large arrays of ligands is often cost-prohibitive due to the high expense of drug discovery functional assays. An analysis of the overlap of 9 PK and 3 DTI datasets used in this study indicates that there is limited overlap between individual PK and DTI datasets, especially when considering overlaps of more than 2 datasets (Figure 2). Similarly, there is limited overlap between PK and DTI datasets, with only 0.7% of all DTI molecules having some PK value overlap. This fragmentation poses a major barrier for researchers aiming to address complex questions that require integrated data, such as those in polypharmacy and drug combination studies.

2.2 Drug Discovery Domain Knowledge

The GO is one of the most widely used resources in bioinformatics, offering structured annotations that describe the functions of genes and proteins across species. However, despite its biological richness, GO has rarely been directly integrated into deep learning models for drug discovery tasks. This underutilization stems partly from the dominance of sequence-based representations, which, although effective, often fail to capture the functional hierarchies and semantic relationships encoded in GO. Motivated by this limitation, we aim to enhance the quality of target protein embeddings by incorporating ontology-based information alongside sequence-level features.

Molecular fingerprints are bit strings that encode the structural information of a molecule, such as the presence or absence of specific chemical groups, atom types, or topological features [35]. Molecular fingerprints offer a versatile representation where different algorithms tailored to capture different aspects of molecular structure, such as key-based fingerprints and hash fingerprints. Key-based fingerprints, including MACCS [36] and RDKit [37], utilize a predefined fragment library to encode each molecule into a binary bit stream according to its substructure. Hash-based fingerprints such as Morgan fingerprints [38] encode substructures in a molecule based on paths around atoms in a molecule. Leveraging fingerprints alongside SMILES representations in parallel increases the generalizability of models [39].

3 Method

xImagand-DKI is an SP2PKDTI diffusion model conditioned on learned SMILES and protein embeddings from their respective encoder models to generate target PK properties and DTI values. xImagand-DKI resembles a typical vision transformer architecture [40]; see Figure 1. 1D patches are computed from the classifier-free guidance of SMILES and protein embeddings and concatenated with PK class tokens. Diffusion step embeddings are generated using sinusoidal position encodings [41]. Patches are then fed alongside sinusoidal step embeddings [42] to a transformer base. As the data is sparse over ligands, we apply masking when computing the loss to flow gradients from known PK and DTI values during training. Exponential Moving Average (EMA) [43] is applied to the base model during training to generate the final model used for sampling. Additional training details about pre-trained encoders and hyperparameters can be found in appendix A.1.

3.1 Diffusion Model

Given samples from a data distribution $q(x_0)$, we are interested in learning a model distribution $p_\theta(x_0)$ that approximates $q(x_0)$ and is easy to sample from. Jonathan et al. [15] considers the following Markov chain with Gaussian transitions parameterized by a decreasing sequence $\alpha_{1:T} \in (0, 1]^T$:

$$q(x_{1:T}|x_0) := \mathcal{N}(x_{1:T}|\sqrt{\alpha_{1:T}}x_0, (1 - \alpha_{1:T})\mathbf{I}) \quad (1)$$

This is called the *forward process*, whereas the latent variable model $p_\theta(x_{0:T})$ is the generative process, approximating the *reverse process* $q(x_{t-1}|x_t)$. The forward process of x_t can be expressed as a linear combination of x_0 and noise variable ϵ :

$$x_t = \sqrt{\alpha_t}x_0 + \sqrt{1 - \alpha_t}\epsilon \quad (2)$$

We train with the simplified objective:

$$L(\epsilon_\theta) := \sum_{t=1}^T \mathbb{E}_{x_0 \sim q(x_0), \epsilon_t} [\|\epsilon_\theta^{(t)}(x_t) - \epsilon_t\|_2^2] \quad (3)$$

where $\epsilon_\theta := \{\epsilon_\theta^{(t)}\}_{t=1}^T$ is a set of T functions, indexed by t , each with trainable parameters $\theta^{(t)}$.

3.2 Infusing Relationships from Gene Ontology

We leverage PO2Vec [44], a recent embedding technique that transforms GO structures into continuous vector representations. Intuitively, PO2Vec relates the similarity between two terms t_i and t_j to the length of the shortest path between t_i and t_j in the GO. PO2Vec defines the shortest path based on three cases: (1) direct reachability $\mathcal{Q}_{dr}(t_i)$, if there exists a directed path starting at t_i and ends at t_j ; (2) indirect reachability $\mathcal{Q}_{ir}(t_i)$, if there exists a term t_k , reachable from both t_i and t_j ; (3) unreachable $\mathcal{Q}_{ur}(t_i)$, if t_i and t_j are neither directly or indirectly reachable from t_i .

PO2Vec applies contrastive learning to learn a partial order by sampling positive samples t_i^+ from $\mathcal{Q}_{dr}(t_i)$ or $\mathcal{Q}_{ir}(t_i)$ with specified shortest path length and k negative samples $\mathcal{N}(t_i)$ from indexed $\mathcal{Q}_{dr}(t_i)$, $\mathcal{Q}_{ir}(t_i)$, and $\mathcal{Q}_{ur}(t_i)$ with greater lengths. With $s(x, y)$ as cosine similarity between x, y , PO2Vec utilizes InfoNCE [45] defined by the following:

$$\mathcal{L}_{GO} = - \sum_{i=1}^m \log \frac{s(t_i, t_i^+)}{\sum_{t_j \in \mathcal{N}(t_i) \cup \{t_i^+\}} s(t_i, t_j)} \quad (4)$$

The resulting GO term embeddings are then aggregated via average pooling over the annotated terms to obtain functional representations of genes. By integrating PO2Vec with ProtBert-derived sequence embeddings prior to the diffusion process, our model benefits from both molecular sequence information and ontology-driven semantics, leading to more biologically meaningful target representations.

3.3 Infusing Structural and Circular Drug Fingerprints

We leverage FPFormer, a novel embedding model pre-trained on both structural and circular fingerprints from ChEMBL [13] and Moses [46]. FPFormer utilizes a novel tokenization methodology that converts different sparse fingerprints into a chemical language and sequence, compatible with masked language modelling pre-training and embedding techniques. Molecular fingerprints can be computed from SMILES strings, where each method looks to represent and encode different aspect of a molecule [47]. We utilize a mixture of structural, circular, and atom-pair fingerprints, to pre-train our FPFormer model to generate meaningful molecular embedding representations, complementary to our SMILES molecular representations. Training data consists of tokenized sparse vectors of molecular fingerprints ECFP4, FCFP6, MACCS, AVALON, TOPTOR, and ATOMPAIR concatenated together. This fingerprint representation, used in parallel to our learned SMILES embeddings, increases the generalizability of our model.

4 Experiments

In the following, we describe the model training details and compare our synthetic data to real data, in terms of machine learning efficiency (MLE) and univariate and bivariate statistical distributions. We then discuss ablation studies and key findings. The metrics for MLE, univariate, and bivariate evaluations are further defined in their respective subsections. We compare Imagand with baselines of Conditional GAN (cGAN) [48] and Syngand [9]. Similar to in Imagand, SMILES-embeddings from a pre-trained T5 model are used conditionally by the cGAN model to generate PK properties as output for a specific drug. Additional baseline results are provided in appendix A.2.

4.1 Pharmacokinetic and Drug-Target Interaction Datasets

All 9 PK and 3 DTI datasets are collected from TDCommons [11]. We select PK datasets suitable for regression from the ADMET categories. We select DTI datasets from BindingDB [49] covering properties such as inhibition constant (K_i), dissociation constant (K_d), and half maximal inhibitory

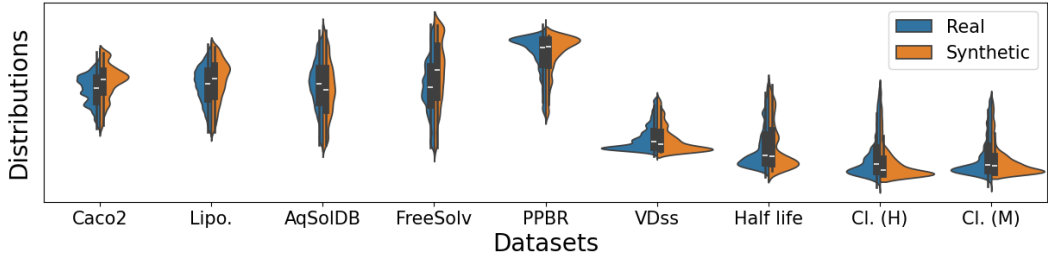


Figure 3: Distributions of ligand PK properties. Blue, synthetic distributions; orange, real distributions.

Model	PKs										DTIs		
	C2	Li.	Aq	FS	PP	VD	HL	CIH	CIM	K_d	K_i	$IC50$	
Sygd	0.62	0.53	0.34	0.50	0.66	0.81	0.85	0.59	0.58	\emptyset	\emptyset	\emptyset	
cGAN	0.19	0.16	0.17	0.18	0.25	0.24	0.28	0.32	0.29	0.32	0.08	0.13	
Imgd	0.19	0.12	0.13	0.18	0.20	0.27	0.36	0.20	0.19	0.27	0.13	0.11	
No DKI	0.12	0.08	0.07	0.13	0.11	0.12	0.15	0.13	0.18	0.26	0.07	0.09	
Ours	0.13	0.07	0.07	0.12	0.09	0.08	0.15	0.15	0.15	0.24	0.06	0.07	

Table 2: Average Hellinger distance across 30 generated synthetic target property datasets for ablation experiment configurations. The best HD values for each ablation test are bolded. We compare our proposed model with and without DKI to existing benchmarks of Imagand, Syngand, and cGAN.

concentration (IC50). Revealing the overlap sparsity between DTI and PK, out of around 700k molecules from BindingDB, only around 5k molecules (0.7%) have PK properties defined from one of the 9 PK datasets.

The **inhibition constant** is a measure of how strongly an inhibitor binds to an enzyme, effectively indicating the inhibitor’s potency. BindingDB has 375k pairs of K_i values from 175k drugs and 3k proteins. The **dissociation constant** quantifies binding affinity between a drug and its target protein, defined as the free ligand concentration at which 50% of the protein binding sites are occupied at equilibrium. BindingDB has 52k pairs of K_d values from 11k drugs and 1.5k proteins. The **half maximal inhibitory concentration** is a measure of the potency of a substance in inhibiting a specific biological or biochemical function. BindingDB has 991k pairs of IC50 values from 550k drugs and 5k proteins.

Caco-2 [50] is an absorption dataset containing rates of 906 drugs passing through the Caco-2 cells, approximating the rate at which the drugs permeate through the human intestinal tissue. **Lipophilicity** [51] is an absorption dataset that measures the ability of 4,200 drugs to dissolve in a lipid (e.g. fats, oils) environment. **AqSolvDB** [52] is an absorption dataset that measures the ability of 9,982 drugs to dissolve in water. **FreeSolv** [53] is an absorption dataset that measures the experimental and calculated hydration-free energy of 642 drugs in water.

Plasma Protein Binding Rate (PPBR) [54] is a distribution dataset of percentages for 1,614 drugs on how they bind to plasma proteins in the blood. **Volume of Distribution at steady state (VDss)** [55] is a distribution dataset that measures the degree of concentration for 1,130 drugs in body tissue compared to their concentration in blood.

Half Life [56] is an excretion dataset for 667 drugs on the duration for the concentration of the drug in the body to be reduced by half. **Clearance** [57] is an excretion dataset for around 1,050 drugs on two clearance experiment types, microsome and hepatocyte. Drug clearance is defined as the volume of plasma cleared of a drug over a specified time [11]. **Acute Toxicity (LD50)** [58] is a toxicity dataset that measures the most conservative dose for 7,385 drugs that can lead to lethal adverse effects.

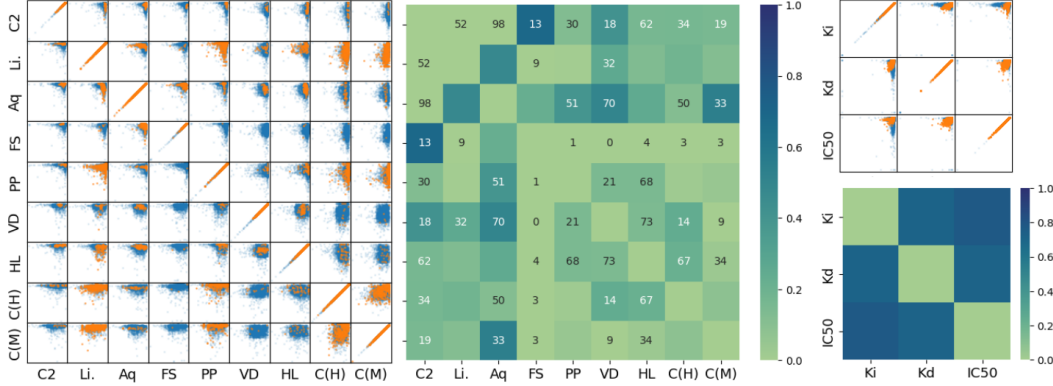


Figure 4: Overview of bivariate comparison between synthetic and real data. We show pairwise scatter plots for pairs of PK and DTI target properties. Real data is marked in orange, and synthetic data is marked in blue. Pairwise combinations with fewer than 100 examples have their cardinality numbered in the heatmaps. The heatmap plots are the Differential Pairwise Correlations (DPC) using Pearson Correlation Coefficient for pairs of PK target properties between real and synthetic data.

4.2 Univariate Comparisons to Real Data

Hellinger distance (HD) quantifies the similarity between two probability distributions and can be used as a summary statistic of differences for each PK target property between real and synthetic datasets. Given two discrete probability distributions $P = \{p_1, p_2, \dots, p_n\}$ and $Q = \{q_1, q_2, \dots, q_n\}$, the HD between P and Q is expressed in Equation 5.

$$HD^2(p, q) = \frac{1}{2} \sum_{i=1}^n (\sqrt{p_i} - \sqrt{q_i})^2 \quad (5)$$

With scores ranging between 0 to 1, HD values closer to 0 indicate smaller differences between real and synthetic data and are thus desirable.

Figure 3 shows the distributions of PK synthetic data generated by xImagand-DKI with the real data. Computing the Hellinger distance, Table 2, we see an average of 0.11, meaning that our model produces synthetic data that closely resembles the distribution of real data. Table 2 shows that data generated from our proposed architecture more closely resembles real data compared to other models. Table 3 shows the results of the PK and DTI regression tasks using real and synthetic augmented datasets. Results of these experiments suggest that a synthetic augmented dataset has equivalent utility as real data over our PK and DTI datasets. Additional tasks will be explored in future work. xImagand-DKI has similar MLE performance compared to cGAN.

4.3 Bivariate Correlations of Synthetic Data

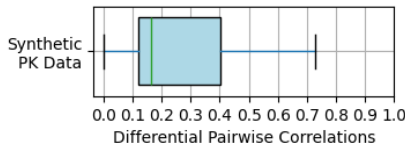


Figure 5: Boxplot of Pairwise correlations

In addition to univariate comparisons, synthetic PK target properties can be compared to real data in terms of bivariate pairwise distributions and correlations. Differential Pairwise Correlations (DPC) provides a multivariate metric for evaluating the quality of synthetic data when compared to real data. We define the DPC as the absolute difference between the bivariate correlation coefficient of real and synthetic data, denoted by subscripts r and s , respectively, as shown in Equation 6.

$$\Delta CV_{cont_{XY}} = |\rho_{XYr} - \rho_{XYS}| \quad (6)$$

where X and Y denote the two continuous variables, whereas ρ_{XY} is the correlation coefficient for X and Y . If the real and synthetic PK target property datasets are highly similar (i.e., the synthetic

		Models						Models			
		Real	cGAN	Imgd	Ours			Real	cGAN	Imgd	Ours
C2	mse	0.63	0.17	0.13	0.06	HL	mse	0.53	0.28	0.26	0.07
	R2	-3.2	-0.08	0.14	-0.13		R2	-1.6	-0.54	-0.28	-0.09
	pcc	0.35	0.34	0.43	0.35		pcc	0.16	0.13	0.03	0.17
Li.	mse	0.17	0.14	0.15	0.09	CH	mse	1.9	0.43	0.43	0.15
	R2	0.04	0.19	0.14	0.01		R2	-4.2	-0.15	-0.20	-0.13
	pcc	0.50	0.47	0.41	0.49		pcc	0.11	0.14	0.10	0.10
Aq	mse	0.075	0.07	0.08	0.07	CM	mse	0.72	0.20	0.21	0.04
	R2	0.56	0.57	0.53	0.38		R2	-2.6	-0.04	-0.04	-0.06
	pcc	0.76	0.76	0.73	0.75		pcc	0.13	0.25	0.25	0.17
FS	mse	0.62	0.20	0.17	0.11	K_d	mse	0.11	0.11	0.11	0.11
	R2	-2.5	-0.09	0.08	-0.22		R2	0.22	0.23	0.23	0.23
	pcc	0.38	0.42	0.39	0.39		pcc	0.50	0.49	0.50	0.50
PP	mse	3.5	0.26	0.26	0.04	K_i	mse	0.11	0.11	0.11	0.11
	R2	-13	-0.08	-0.06	-0.05		R2	0.21	0.21	0.22	0.22
	pcc	0.10	0.23	0.22	0.10		pcc	0.46	0.46	0.47	0.47
VD	mse	0.54	0.21	0.20	0.04	I50	mse	0.13	0.13	0.13	0.13
	R2	-1.8	-0.06	-0.02	-0.07		R2	0.16	0.16	0.16	0.16
	pcc	0.23	0.31	0.30	0.21		pcc	0.40	0.40	0.40	0.40

Table 3: Comparing drug discovery Machine Learning Efficiency (MLE) regression performances between different models and with real train data. Mean Squared Error (mse), R-Squared (R2), and Pearson Correlation Coefficient (pcc) values are averaged over 30 trials, with the best scores on the real testset bolded. R2 and pcc values are scale-adjusted relative to Real-Real with cGAN and Imagand results.

dataset closely resembles the real dataset), then the absolute difference would be close to 0 or very small, as seen in Figure 5. Heatmaps in Figure 4 show DPC on the Pearson correlation coefficient (pcc) between both PK and DTI data points. Many pairwise combinations of PK target properties have very few overlapping real data values, and pairwise combinations with fewer than 100 examples have their cardinality numbered in the heatmaps in Figure 4. We omit DPC values for pairwise combinations with cardinality less than 10. These results indicate that the generated synthetic PK target properties resemble real data in pairwise correlations.

4.4 Performance on Real-World Tasks

Machine Learning Efficiency (MLE) is a measure that assesses the ability of the synthetic data to replicate a specific use case [59–61]. MLE represents the ability of the synthetic data to replace or augment real data in downstream use cases. To measure MLE, two linear regression models are trained separately, one with synthetic and the other with real data. Then their performance is compared using Mean-Squared Error (mse), R-Squared (R2), and Pearson Correlation Coefficient (pcc), is evaluated on real data test sets. Each linear regression model is trained using T5 chemical and ProtBERT embeddings to predict each PK and DTI target property value.

To ensure an adequately sized test set (>300 ligands, i.e. >10% size of our synthetic data) to evaluate our downstream models, we divide real data into segments A_r and B_r using a 50%/50% split. To ensure a synthetic test set similar in size to real data test sets (~ 300 ligands), we divide synthetic data into segments A_s and B_s using a 90%/10% split. The real train set is defined as A_r , and the real test set is defined as B_r . The augmented train set is defined as $A_r \cup A_s$, and the augmented test set is defined as $B_r \cup B_s$. Outliers are removed from both real and augmented train and test sets based on $Q1 - 1.5IQR$ lower and $Q3 + 1.5IQR$ upper bounds on the synthetic data.

Table 3 shows the results of the PK regression tasks using real and synthetic augmented datasets. Results of these experiments suggest that a synthetic augmented dataset can outperform real data

with statistical significance over many PK datasets. Additional tasks will be explored in future work. We see that synthetic data from both cGAN and Imagand can improve MLE over using only the real data. Imagand has similar or superior MLE performance compared to cGAN.

5 Limitations and Future Work

Our work is a major step towards building a new class of foundational models for drug discovery trained over a diverse range of datasets. Given the problem of data overlap sparsity, xImagand-DKI can be utilized primarily as a *in silico* pre-clinical tool, aimed to reduce the costs of *in vitro* experiments and high-throughput screening. As a research tool, scientists can utilize our models to investigate and generate properties for novel molecules to be used for downstream PBPK simulations without costly assays. Even as an initial step, xImagand-DKI has many real-world pre-clinical applications where data overlap sparsity and data scarcity are challenges.

- **Limited applicability to *in vivo* applications.** Although we cover a wide variety of ADMET and DTI datasets, most of these datasets are *in vitro*. *In vivo* experiments provides real-world data that complements *in vitro* studies, where that data can be used to further improve the performance of our models.
- **Applicability only to numerical drug discovery datasets.** With the limitations of our diffusion methods, we are restricted to utilizing only numerical datasets. This limits the types of datasets that our model is applicable with, such as ToxCast [62] classification datasets of over 600 experiments.
- **Extending beyond PK/DTI drug discovery tasks.** PK/DTI data and research makes up only a small section of pre-clinical drug-discovery. AI for lead optimization, de novo drug design, and protein-docking are other interconnected research innovating pre-clinical drug discovery.

Future work will look to extend our model to *in vivo* datasets and investigate how our generated data can be used for quantitative *in vitro*-to-*in vivo* extrapolation. We will look to extend our model to categorical diffusion methods as well as investigating integration with other drug discovery tasks in lead optimization, de novo generation, and protein-docking. Extending our model to categorical datasets and other drug discovery tasks will allow us to benchmark and train our model on additional drug discovery datasets, adaptable for a larger number of tasks.

6 Conclusions

The SMILES/Protein to PK/DTI model xImagand-DTI generates synthetic PK and DTI target property data that closely resembles real data in univariate and for downstream tasks. xImagand-DKI provides a solution for the challenge of sparse overlapping PK and DTI target property data, allowing researchers to generate data to tackle complex research questions and for high-throughput screening. Future work will expand xImagand-DKI to categorical PK and DTI properties, and scale to more datasets and larger model sizes. For future work, we will look to extend our model to include *in vivo* datasets and to investigate new applications of xImagand-DKI for QIVIVE.

References

- [1] Jintae Kim, Sera Park, Dongbo Min, and Wankyu Kim. Comprehensive survey of recent drug discovery using deep learning. *International Journal of Molecular Sciences*, 22(18):9983, 2021.
- [2] Olivier J Wouters, Martin McKee, and Jeroen Luyten. Estimated research and development investment needed to bring a new medicine to market, 2009-2018. *Jama*, 323(9):844–853, 2020.
- [3] Steven M Paul, Daniel S Mytelka, Christopher T Dunwiddie, Charles C Persinger, Bernard H Munos, Stacy R Lindborg, and Aaron L Schacht. How to improve r&d productivity: the pharmaceutical industry’s grand challenge. *Nature reviews Drug discovery*, 9(3):203–214, 2010.
- [4] Ankita Murmu and Balázs Győrffy. Artificial intelligence methods available for cancer research. *Frontiers of Medicine*, pages 1–20, 2024.

[5] Maha A Thafar, Mona Alshahrani, Somayah Albaradei, Takashi Gojobori, Magbubah Essack, and Xin Gao. Affinity2vec: drug-target binding affinity prediction through representation learning, graph mining, and machine learning. *Scientific reports*, 12(1):4751, 2022.

[6] Jong-Hoon Park and Young-Rae Cho. DRAW+: network-based computational drug repositioning with attention walking and noise filtering. *Health Information Science and Systems*, 13(1):14, 2025.

[7] Majun Lian, Wenli Du, Xinjie Wang, and Qian Yao. Drug-target interaction prediction based on multi-similarity fusion and sparse dual-graph regularized matrix factorization. *IEEE Access*, 9: 99718–99730, 2021.

[8] Clement Vignac, Igor Krawczuk, Antoine Siraudin, Bohan Wang, Volkan Cevher, and Pascal Frossard. Digress: Discrete denoising diffusion for graph generation, 2023.

[9] Bing Hu, Ashish Saragadam, Anita Layton, and Helen Chen. Synthetic data from diffusion models improve drug discovery prediction, 2024. URL <https://arxiv.org/abs/2405.03799>.

[10] Bing Hu, Anita Layton, and Helen Chen. Drug discovery smiles-to-pharmacokinetics diffusion models with deep molecular understanding, 2025. URL <https://arxiv.org/abs/2408.07636>.

[11] Kexin Huang, Tianfan Fu, Wenhao Gao, Yue Zhao, Yusuf Roohani, Jure Leskovec, Connor W. Coley, Cao Xiao, Jimeng Sun, and Marinka Zitnik. Therapeutics data commons: Machine learning datasets and tasks for drug discovery and development, 2021.

[12] Nathan Brown, Marco Fiscato, Marwin H.S. Segler, and Alain C. Vaucher. Guacamol: Benchmarking models for de novo molecular design. *Journal of Chemical Information and Modeling*, 59(3):1096–1108, 2019. doi: 10.1021/acs.jcim.8b00839. URL <https://doi.org/10.1021/acs.jcim.8b00839>. PMID: 30887799.

[13] Anna Gaulton, Anne Hersey, Michał Nowotka, A Patricia Bento, Jon Chambers, David Mendez, Prudence Mutwo, Francis Atkinson, Louisa J Bellis, Elena Cibrián-Uhalte, et al. The chembl database in 2017. *Nucleic acids research*, 45(D1):D945–D954, 2017.

[14] Silvia Scoarta, Asli Küçükosmanoglu, Felix Bindt, Marianne Pouwer, and Bart A Westerman. A roadmap to use nonstructured data to discover multitarget cancer therapies. *JCO clinical cancer informatics*, 7:e2200096, 2023.

[15] Ho Jonathan, Jain Ajay, and Abbeel Pieter. Denoising diffusion probabilistic models, 2020.

[16] Zhiye Guo, Jian Liu, Yanli Wang, Mengrui Chen, Duolin Wang, Dong Xu, and Jianlin Cheng. Diffusion models in bioinformatics and computational biology. *Nature Reviews Bioengineering*, pages 1–19, 2023.

[17] Lemeng Wu, Chengyue Gong, Xingchao Liu, Mao Ye, and Qiang Liu. Diffusion-based molecule generation with informative prior bridges, 2022.

[18] Ilia Igashov, Hannes Stärk, Clément Vignac, Victor Garcia Satorras, Pascal Frossard, Max Welling, Michael Bronstein, and Bruno Correia. Equivariant 3d-conditional diffusion models for molecular linker design, 2022.

[19] Parthasarathy Suryanarayanan, Yunguang Qiu, Shreyans Sethi, Diwakar Mahajan, Hongyang Li, Yuxin Yang, Elif Eyigoz, Aldo Guzman Saenz, Daniel E. Platt, Timothy H. Rumbell, Kenney Ng, Sanjoy Dey, Myson Burch, Bum Chul Kwon, Pablo Meyer, Feixiong Cheng, Jianying Hu, and Joseph A. Morrone. Multi-view biomedical foundation models for molecule-target and property prediction, 2025. URL <https://arxiv.org/abs/2410.19704>.

[20] Shihao Ma, Andy G. X. Zeng, Benjamin Haibe-Kains, Anna Goldenberg, John E Dick, and Bo Wang. Integrate any omics: Towards genome-wide data integration for patient stratification, 2024. URL <https://arxiv.org/abs/2401.07937>.

[21] Suzi A Aleksander, James Balhoff, Seth Carbon, J Michael Cherry, Harold J Drabkin, Dustin Ebert, Marc Feuermann, Pascale Gaudet, Nomi L Harris, et al. The gene ontology knowledge-base in 2023. *Genetics*, 224(1):iyad031, 2023.

[22] Han Huang, Leilei Sun, Bowen Du, and Weifeng Lv. Conditional diffusion based on discrete graph structures for molecular graph generation, 2023.

[23] Emiel Hoogeboom, Victor Garcia Satorras, Clément Vignac, and Max Welling. Equivariant diffusion for molecule generation in 3d, 2022.

[24] Victor Garcia Satorras, Emiel Hoogeboom, Fabian B. Fuchs, Ingmar Posner, and Max Welling. E(n) equivariant normalizing flows for molecule generation in 3d. *CoRR*, abs/2105.09016, 2021. URL <https://arxiv.org/abs/2105.09016>.

[25] Qiao Ning, Yue Wang, Yaomiao Zhao, Jiahao Sun, Lu Jiang, Kaidi Wang, and Minghao Yin. Dmhgnn: Double multi-view heterogeneous graph neural network framework for drug-target interaction prediction. *Artificial Intelligence in Medicine*, 159:103023, 2025.

[26] Mingyang Wang, Chang-Yu Hsieh, Jike Wang, Dong Wang, Gaoqi Weng, Chao Shen, Xiaojun Yao, Zhitong Bing, Honglin Li, Dongsheng Cao, et al. Relation: A deep generative model for structure-based de novo drug design. *Journal of Medicinal Chemistry*, 65(13):9478–9492, 2022.

[27] James P Hughes, Stephen Rees, S Barrett Kalindjian, and Karen L Philpott. Principles of early drug discovery. *British journal of pharmacology*, 162(6):1239–1249, 2011.

[28] Yohei Kawabata, Koichi Wada, Manabu Nakatani, Shizuo Yamada, and Satomi Onoue. Formulation design for poorly water-soluble drugs based on biopharmaceutics classification system: Basic approaches and practical applications. *International Journal of Pharmaceutics*, 420(1):1–10, 2011. ISSN 0378-5173. doi: <https://doi.org/10.1016/j.ijpharm.2011.08.032>. URL <https://www.sciencedirect.com/science/article/pii/S0378517311007940>.

[29] Dixit V. Bhalani, Bhingaradiya Nutan, Avinash Kumar, and Arvind K. Singh Chandel. Bioavailability enhancement techniques for poorly aqueous soluble drugs and therapeutics. *Biomedicines*, 10(9), 2022. ISSN 2227-9059. doi: 10.3390/biomedicines10092055. URL <https://www.mdpi.com/2227-9059/10/9/2055>.

[30] I Kola. The state of innovation in drug development. *Clinical pharmacology and therapeutics*, 83:227–30, 02 2008. doi: 10.1038/sj.cpt.6100479.

[31] Michael J. Waring, John Edmund Arrowsmith, Andrew R. Leach, Paul D. Leeson, Sam Mandrell, Robert M. Owen, Garry Pairaudeau, William D. Pennie, Stephen D. Pickett, Jibo Wang, Owen Wallace, and Alexander Weir. An analysis of the attrition of drug candidates from four major pharmaceutical companies. *Nature Reviews Drug Discovery*, 14:475–486, 2015. URL <https://api.semanticscholar.org/CorpusID:25292436>.

[32] Michael Davies, Rhys D.O. Jones, Ken Grime, Rasmus Jansson-Löfmark, Adrian J. Fretland, Susanne Winiwarter, Paul Morgan, and Dermot F. McGinnity. Improving the accuracy of predicted human pharmacokinetics: Lessons learned from the astrazeneca drug pipeline over two decades. *Trends in Pharmacological Sciences*, 41(6):390–408, 2020. ISSN 0165-6147. doi: <https://doi.org/10.1016/j.tips.2020.03.004>. URL <https://www.sciencedirect.com/science/article/pii/S0165614720300687>.

[33] Sameed Ahmed, Jennifer C Sullivan, and Anita T Layton. Impact of sex and pathophysiology on optimal drug choice in hypertensive rats: quantitative insights for precision medicine. *Iscience*, 24(4), 2021.

[34] Heba Askr, Enas Elgeldawi, Heba Aboul Ella, Yaseen AMM Elshaier, Mamdouh M Gomaa, and Aboul Ella Hassanien. Deep learning in drug discovery: an integrative review and future challenges. *Artificial Intelligence Review*, 56(7):5975–6037, 2023.

[35] Wenhao Hu, Yingying Liu, Xuanyu Chen, Wenhao Chai, Hangyue Chen, Hongwei Wang, and Gaoang Wang. Deep learning methods for small molecule drug discovery: A survey. *IEEE Transactions on Artificial Intelligence*, 5(2):459–479, 2023.

[36] Joseph L Durant, Burton A Leland, Douglas R Henry, and James G Nourse. Reoptimization of mdl keys for use in drug discovery. *Journal of chemical information and computer sciences*, 42(6):1273–1280, 2002.

[37] Greg Landrum. Rdkit documentation. *Release*, 1(1-79):4, 2013.

[38] Harry L Morgan. The generation of a unique machine description for chemical structures-a technique developed at chemical abstracts service. *Journal of chemical documentation*, 5(2):107–113, 1965.

[39] Johannes Schimunek, Philipp Seidl, Lukas Friedrich, Daniel Kuhn, Friedrich Rippmann, Sepp Hochreiter, and Günter Klambauer. Context-enriched molecule representations improve few-shot drug discovery. *arXiv preprint arXiv:2305.09481*, 2023.

[40] Alexey Dosovitskiy, Lucas Beyer, Alexander Kolesnikov, Dirk Weissenborn, Xiaohua Zhai, Thomas Unterthiner, Mostafa Dehghani, Matthias Minderer, Georg Heigold, Sylvain Gelly, Jakob Uszkoreit, and Neil Houlsby. An image is worth 16x16 words: Transformers for image recognition at scale, 2021. URL <https://arxiv.org/abs/2010.11929>.

[41] Ashish Vaswani, Noam Shazeer, Niki Parmar, Jakob Uszkoreit, Llion Jones, Aidan N. Gomez, Łukasz Kaiser, and Illia Polosukhin. Attention is all you need, 2023. URL <https://arxiv.org/abs/1706.03762>.

[42] Jonathan Ho, Chitwan Saharia, William Chan, David J. Fleet, Mohammad Norouzi, and Tim Salimans. Cascaded diffusion models for high fidelity image generation, 2021. URL <https://arxiv.org/abs/2106.15282>.

[43] Antti Tarvainen and Harri Valpola. Mean teachers are better role models: Weight-averaged consistency targets improve semi-supervised deep learning results, 2018. URL <https://arxiv.org/abs/1703.01780>.

[44] Wenjing Li, Bin Wang, Jin Dai, Yan Kou, Xiaojun Chen, Yi Pan, Shuangwei Hu, and Zhenjiang Zech Xu. Partial order relation-based gene ontology embedding improves protein function prediction. *Briefings in Bioinformatics*, 25(2):bbae077, 2024.

[45] Aaron van den Oord, Yazhe Li, and Oriol Vinyals. Representation learning with contrastive predictive coding, 2019. URL <https://arxiv.org/abs/1807.03748>.

[46] Daniil Polykovskiy, Alexander Zhebrak, Benjamin Sanchez-Lengeling, Sergey Golovanov, Oktai Tatanov, Stanislav Belyaev, Rauf Kurbanov, Aleksey Artamonov, Vladimir Aladinskiy, Mark Veselov, et al. Molecular sets (moses): a benchmarking platform for molecular generation models. *Frontiers in pharmacology*, 11:565644, 2020.

[47] Adrià Cereto-Massagué, María José Ojeda, Cristina Valls, Miquel Mulero, Santiago García-Vallvé, and Gerard Pujadas. Molecular fingerprint similarity search in virtual screening. *Methods*, 71:58–63, 2015.

[48] Mehdi Mirza and Simon Osindero. Conditional generative adversarial nets. *arXiv preprint arXiv:1411.1784*, 2014.

[49] Tiqing Liu, Yuhmei Lin, Xin Wen, Robert N Jorissen, and Michael K Gilson. Bindingdb: a web-accessible database of experimentally determined protein–ligand binding affinities. *Nucleic acids research*, 35(suppl_1):D198–D201, 2007.

[50] Ning-Ning Wang, Jie Dong, Yin-Hua Deng, Minfeng Zhu, Ming Wen, Zhiqiang Yao, Aiping Lu, Jianbing Wang, and Dongsheng Cao. Adme properties evaluation in drug discovery: Prediction of caco-2 cell permeability using a combination of nsga-ii and boosting. *Journal of chemical information and modeling*, 56(4):763–73, 2016. URL <https://api.semanticscholar.org/CorpusID:206609089>.

[51] Zhenqin Wu, Bharath Ramsundar, Evan N Feinberg, Joseph Gomes, Caleb Geniesse, Aneesh S Pappu, Karl Leswing, and Vijay Pande. Moleculenet: a benchmark for molecular machine learning. *Chemical science*, 9(2):513–530, 2018.

[52] Murat Cihan Sorkun, Abhishek Khetan, and Süleyman Er. Aqsoldb, a curated reference set of aqueous solubility and 2d descriptors for a diverse set of compounds. *Scientific data*, 6(1):143, 2019.

[53] David L Mobley and J Peter Guthrie. Freesolv: a database of experimental and calculated hydration free energies, with input files. *Journal of computer-aided molecular design*, 28: 711–720, 2014.

[54] Mark Wenlock and Nicholas Tomkinson. Experimental in vitro dmpk and physicochemical data on a set of publicly disclosed compounds. *CHEMBL*, 2016. doi: 10.6019/CHEMBL3301361.

[55] Franco Lombardo and Yankang Jing. In silico prediction of volume of distribution in humans. extensive data set and the exploration of linear and nonlinear methods coupled with molecular interaction fields descriptors. *Journal of chemical information and modeling*, 56(10):2042–2052, 2016.

[56] R Scott Obach, Franco Lombardo, and Nigel J Waters. Trend analysis of a database of intravenous pharmacokinetic parameters in humans for 670 drug compounds. *Drug Metabolism and Disposition*, 36(7):1385–1405, 2008.

[57] Li Di, Christopher Keefer, Dennis O Scott, Timothy J Strelevitz, George Chang, Yi-An Bi, Yurong Lai, Jonathon Duckworth, Katherine Fenner, Matthew D Troutman, et al. Mechanistic insights from comparing intrinsic clearance values between human liver microsomes and hepatocytes to guide drug design. *European journal of medicinal chemistry*, 57:441–448, 2012.

[58] Hao Zhu, Todd M Martin, Lin Ye, Alexander Sedykh, Douglas M Young, and Alexander Tropsha. Quantitative structure- activity relationship modeling of rat acute toxicity by oral exposure. *Chemical research in toxicology*, 22(12):1913–1921, 2009.

[59] Fida K Dankar and Mahmoud Ibrahim. Fake it till you make it: Guidelines for effective synthetic data generation. *Applied Sciences*, 11(5):2158, 2021.

[60] Mohammad Ahmed Basri, Bing Hu, Abu Yousuf Md Abdullah, Shu-Feng Tsao, Zahid Butt, and Helen Chen. A hyperparameter tuning framework for tabular synthetic data generation methods. *Journal of Computational Vision and Imaging Systems*, 9(1):76–79, 2023.

[61] Vadim Borisov, Kathrin Seßler, Tobias Leemann, Martin Pawelczyk, and Gjergji Kasneci. Language models are realistic tabular data generators. *arXiv preprint arXiv:2210.06280*, 2022.

[62] Ann M Richard, Richard S Judson, Keith A Houck, Christopher M Grulke, Patra Volarath, Inthirany Thillainadarajah, Chihae Yang, James Rathman, Matthew T Martin, John F Wambaugh, et al. Toxcast chemical landscape: paving the road to 21st century toxicology. *Chemical research in toxicology*, 29(8):1225–1251, 2016.

[63] Seyone Chithrananda, Gabriel Grand, and Bharath Ramsundar. Chemberta: Large-scale self-supervised pretraining for molecular property prediction, 2020.

[64] Walid Ahmad, Elana Simon, Seyone Chithrananda, Gabriel Grand, and Bharath Ramsundar. Chemberta-2: Towards chemical foundation models. *arXiv preprint arXiv:2209.01712*, 2022.

[65] Sheng Wang, Yuzhi Guo, Yuhong Wang, Hongmao Sun, and Junzhou Huang. Smiles-bert: Large scale unsupervised pre-training for molecular property prediction. *Proceedings of the 10th ACM International Conference on Bioinformatics, Computational Biology and Health Informatics*, 2019. URL <https://api.semanticscholar.org/CorpusID:202159174>.

[66] Viraj Bagal, Rishal Aggarwal, PK Vinod, and U Deva Priyakumar. Molgpt: molecular generation using a transformer-decoder model. *Journal of Chemical Information and Modeling*, 62(9): 2064–2076, 2021.

[67] Ahmed Elnaggar, Michael Heinzinger, Christian Dallago, Ghalia Rehawi, Yu Wang, Llion Jones, Tom Gibbs, Tamas Feher, Christoph Angerer, Martin Steinegger, DEBSINDHU BHOWMIK, and Burkhard Rost. Prottrans: Towards cracking the language of life’s code through self-supervised deep learning and high performance computing. *bioRxiv*, 2020. doi: 10.1101/2020.07.12.199554. URL <https://www.biorxiv.org/content/early/2020/07/21/2020.07.12.199554>.

- [68] Thomas Wolf, Lysandre Debut, Victor Sanh, Julien Chaumond, Clement Delangue, Anthony Moi, Pierrick Cistac, Tim Rault, Rémi Louf, Morgan Funtowicz, Joe Davison, Sam Shleifer, Patrick von Platen, Clara Ma, Yacine Jernite, Julien Plu, Canwen Xu, Teven Le Scao, Sylvain Gugger, Mariama Drame, Quentin Lhoest, and Alexander M. Rush. Transformers: State-of-the-art natural language processing. In *Proceedings of the 2020 Conference on Empirical Methods in Natural Language Processing: System Demonstrations*, pages 38–45, Online, October 2020. Association for Computational Linguistics. URL <https://www.aclweb.org/anthology/2020.emnlp-demos.6>.
- [69] Chitwan Saharia, William Chan, Saurabh Saxena, Lala Li, Jay Whang, Emily Denton, Seyed Kamyar Seyed Ghasemipour, Burcu Karagol Ayan, S. Sara Mahdavi, Rapha Gontijo Lopes, Tim Salimans, Jonathan Ho, David J Fleet, and Mohammad Norouzi. Photorealistic text-to-image diffusion models with deep language understanding, 2022.
- [70] Prafulla Dhariwal and Alex Nichol. Diffusion models beat gans on image synthesis, 2021. URL <https://arxiv.org/abs/2105.05233>.
- [71] Jonathan Ho and Tim Salimans. Classifier-free diffusion guidance, 2022. URL <https://arxiv.org/abs/2207.12598>.
- [72] Nitish Srivastava, Geoffrey Hinton, Alex Krizhevsky, Ilya Sutskever, and Ruslan Salakhutdinov. Dropout: A simple way to prevent neural networks from overfitting. *Journal of Machine Learning Research*, 15(56):1929–1958, 2014. URL <http://jmlr.org/papers/v15/srivastava14a.html>.

A Appendix

A.1 Training Details

A.1.1 Pre-trained SMILES and Protein Encoders

SP2PKDTI diffusion models need powerful semantic SMILE and protein encoders to capture the complexity of arbitrary chemical and biological structure inputs. Given the sparsity and small size of PK datasets, encoders trained on specific SMILES-Pharmacokinetic or SMILES-Protein pairs are infeasible [11]. Many transformer-based foundational models such as ChemBERTa [63, 64], SMILES-BERT [65], and MOLGPT [66] have been pre-trained to deeply understand molecular and chemical structures and properties. Similar transformer-based foundation models such as ProtBERT [67] have been pre-trained to deeply understand protein structures and properties. After pre-training, these foundational models can then be fine-tuned for various downstream molecular and protein tasks.

We test SMILES embeddings from ChemBERTa [64] and protein embeddings from ProtBERT [67], trained on SMILES-only and protein-only corpora, respectively. Both embedding models were collected through the Huggingface [68] Model Hub. Similar to Saharia et al. [69], we freeze the weights of our embedding models. Because embeddings are computed offline, freezing the weights minimizes computation and memory footprint for embeddings during model training.

Imagand Model		Diffusion Training	
Layers	12	Learning Rate	1e-3
Heads	16	Weight Decay	5e-2
MLP Dim.	768	Epoch	3000
Emb. Dropout	10%	Batch Size	256
Num Patches	48	Warmup	200
Drug Emb. Size	768	Timesteps (Train)	2000
Time Emb. Size	64	Timesteps (Infer.)	150
PK Emb. Size	256	EMA Gamma (γ)	0.994
Prot Emb. Size	1024		
Drug DKI Emb.	768		
Prot DKI Emb.	256		

Table 4: List of Imagand Model Hyperparameters used across experiments. Model hyperparameters include the number of layers, heads, multilayered perceptron (MLP) size, embedding dropout, and sizes for the conditional, time, and pharmacokinetic (Y) embeddings. Training hyperparameters include the learning rate, weight decay, number of epochs, batch size, warmup, diffusion timesteps used for training and inference, and the Exponential Moving Average (EMA) Gamma (γ).

We train a 19M parameter model for S2PK synthesis. Model hyperparameters were not optimized and are described in Table 4. We do not find overfitting to be an issue. For classifier-free guidance, we joint-train unconditionally via dropout zeroing out sections of the SMILES embeddings with 10% probability for all of our models. For the machine learning efficiency, and univariate and bivariate distribution analysis, we utilize DeBERTa embeddings trained on PubChem and DLGN for infilling and as the noise model. We compare our model configuration to other possible configurations in the ablation experiments. All experiments were conducted using a single NVIDIA GeForce RTX 3090 GPU.

A.1.2 Static Thresholding

We apply elementwise clipping the PK predictions to $[-1, 1]$ as static thresholding, similar to Jonathan et al. [15], Saharia et al. [69]. Since PK data is min-max scaled to the same $[-1, 1]$ range as a preprocessing step, static thresholding is essential to prevent the generation of invalid and out-of-range PK values.

A.1.3 Data Processing

We first merge all 9 PK datasets to create a unified dataset containing 17k drugs over 9 unique PK columns for training and testing (90%/10% split) our models. We merge all data from 3 DTI datasets,

to create a unified dataset containing 1.2M drug-protein pairs with 3 dti columns for training and testing (90%/10% split) for our models. Data from 3 DTI datasets are log-transformed. All PK and DTI data are collected from TDCommons [11].

We apply a Gaussian Quantile Transform to both PK and DTI datasets before min-max scaling between the range of $[-1, 1]$. After removing outliers ($Q1 - 1.5\text{IQR}$ lower and $Q3 + 1.5\text{IQR}$ upper bound), we are left with 16.5k drugs from the original 17K drugs and 1.1M pairs from 1.2M DTI pairs. Outliers are removed to ensure that Min-Max normalization does not cause unwarranted skewness in our trainset distribution, causing issues for model training. Before infilling null values using inverse transform sampling, we store the null masks for each drug for the masked loss function.

A.1.4 Hyperparameters

A.1.5 Classifier-free Guidance

Classifier guidance uses gradients from a pre-trained model to improve quality while reducing diversity in conditional diffusion models during sampling [70]. Classifier-free guidance [71] is an alternative technique that avoids this pre-trained model by jointly training a diffusion model on conditional and unconditional objectives via dropping the condition (i.e. with 10% probability). We condition all diffusion models on learned SMILES embedding and sinusoidal time embeddings using classifier-free guidance through dropout [71, 72].

A.2 Ablation Studies

We compare Imagand with a baseline in Conditional GAN (cGAN) [48] with 1.8M parameters and Syngand [9] with 9M parameters. Similar to in Imagand, SMILES-embeddings from a pre-trained T5 model are used conditionally by the cGAN model to generate PK properties as output for a specific drug. Compared to earlier results, Table 5, Figure 7, and Figure 6 shows that Imagand is able to generate more realistic synthetic data compared to cGAN and Syngand.

Data	Mean					Std				
	Real	Ours	Imgd	cGAN	Sygd	Real	Ours	Imgd	cGAN	Sygd
Caco2	0.12	0.13	0.14	0.14	0.58	0.39	0.39	0.38	0.27	0.12
Lipo	0.18	0.19	0.18	0.20	0.62	0.42	0.41	0.39	0.30	0.19
AqSol	0.11	0.18	0.11	0.13	0.10	0.41	0.39	0.36	0.29	0.18
FreeSolv	0.10	0.17	0.12	0.10	0.27	0.42	0.42	0.40	0.29	0.13
PPBR	0.57	0.59	0.56	0.63	0.97	0.50	0.49	0.47	0.37	0.09
VDss	-0.60	-0.61	-0.62	-0.66	-0.98	0.44	0.43	0.39	0.31	0.06
Halflife	-0.56	-0.60	-0.56	-0.61	-0.98	0.45	0.43	0.42	0.32	0.06
CIH	-0.55	-0.58	-0.56	-0.59	-0.97	0.61	0.56	0.55	0.47	0.09
CIM	-0.67	-0.69	-0.68	-0.74	-0.98	0.45	0.44	0.38	0.31	0.06

Table 5: Comparing mean and standard deviation values between real and synthetic target property values, rounded to two significant figures.

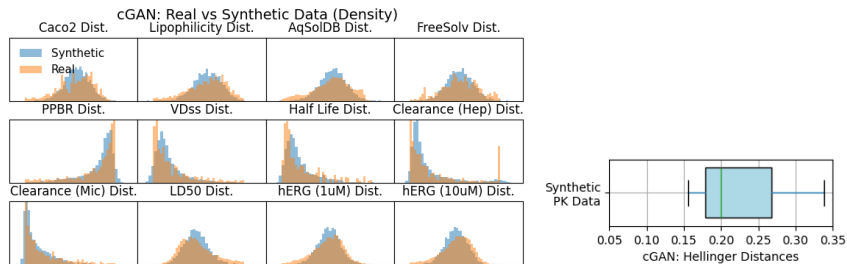


Figure 6: Distributions of ligand PK properties and synthetic PK Data Hellinger Distances (HDS) for cGAN. Blue, synthetic distributions; orange, real distributions.

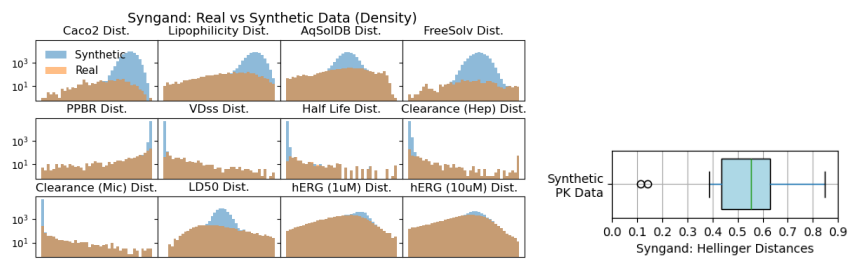


Figure 7: Distributions of ligand PK properties (log-scale) and synthetic PK Data Hellinger Distances (HDs) for Syngand. Blue, synthetic distributions; orange, real distributions.